Nanoscale

COMMUNICATION

Boosting electrochemical oxygen reduction activity of hemoglobin using fructose@graphene-oxide nanoplatforms

Received 00th January 20xx,
Accepted 00th January 20xx

DOI: 10.1039/x0xx00000x

www.rsc.org/

Ana Franco,[a] Manuel Cano,[b*] Juan J. Giner-Casares,[b] E Rodríguez-Castellón,[c] Rafael Luque[a*] and Alain R. Puente-Santiago[a*]

A metal-free oxygen reduction reaction (ORR) electrocatalyst with oustanding performance was obtained through an easy and one-pot synthesis of hemoglobin functionalized fructuose@graphene-oxide (GO) nanocomposites. The active pyridinic nitrogen sites of the highly unfolded enzymes together with the excellent electronic properties of GO appears to be the main factors of the improved electrocatalytic activity.

Findings on the development of high-performances non-platinum electrocatalysts to construct renewable and low-cost electrochemical energy devices such as fuel cells are gaining an increasing impact in the modern society.[1] One of the most attractive alternatives is based on the design of metal-free ORR electrocatalysts, in which a number of drawbacks of Pt-based electrocatalysts including acute poisoning effects (particularly in contact with CO and methanol), low durability and poor scale up, are totally avoided.[2] In recent years, a number of endeavours have been focused on the fabrication of nitrogen-doped carbon nanomaterials that have demonstrated excellent performances and outstanding long-term stabilities,[3-5] in some cases, even comparable or higher than the commercial Pt/C electrocatalysts.[6, 7]

The synthesis of N-doped carbon materials to generate high performances electrocatalytic systems is commonly performed by heating at hard conditions (high temperatures and inert atmosphere) N-rich sources such as pyrrole,[8] aniline,[9] dopamine,[10] urea,[11] among others. These artificial materials usually contains high amount of pyridinic N atoms which greatly influence ORR electrocatalytic yields. In this direction, Junji Nakamura and coworkers have recently updated the recent advances on the understanding of active pyridinic N sites role over the ORR mechanism. They have stated that nitrogen doped carbon nanomaterials are able to create highly efficient ORR electrocatalytic sites owed to carbon atoms close to them act like Lewis bases favouring the adsorption of O_2 molecules.[12] Consequently, the development of easy methodologies to improve the practical applications of the aforementioned materials is still being one of the hottest topics in the energy materials field. In this sense, Nature offers a number of biological materials (enzymes, proteins, etc.) which contain histidines which could be used as natural sources of "pyridine-like" nitrogens providing catalytically active sites for oxygen reduction reactions. Among them, hemoglobin is a tetrameric redox protein formed by four polypeptide chains in which each polypeptide domain encloses at least one iron active redox center. Importantly, each iron redox center is coordinated to the peptide domains by the imidazole ring of both histidine 93 and histidine 64 (through an hydrogen bonding interaction) on the proximal and distal side of the heme pocket, respectively.[13]

In this work, we put forward an unprecedented bottom-up approach to design a high-performance bioelectrocatalytic system from the covalent anchorage of hemoglobin to fructuose modified GO nanoplatforms (GO-Fruc) via glycosylation reaction process. The resulting nanobiomaterials were synthesized at room temperature (GO-Fruc@Hb-RT) and 80ºC (GO-Fruc@Hb-HT) (Scheme 1) in order to get insights on the structural properties of the redox enzymes in both nanocomposites as well as their electrocatalytic function toward ORR reactions.

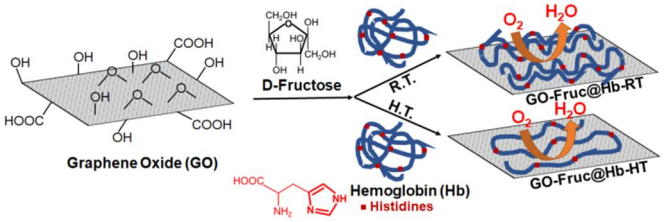

Scheme1. One-pot synthesis of GO-Fruc@Hb nanocomposites.

[a] Departamento de Química Orgánica, Facultad de Ciencias, Universidad de Córdoba, Campus de Rabanales, Ed. Marie Curie, E-14071 Córdoba, Spain. email: rafael.luque@uco.es, z02pusaa@uco.es
[b] Departamento de Química Física y Termodinámica Aplicada, Instituto Universitario de Investigación en Química Fina y Nanoquímica IUIQFN, Facultad de Ciencias, Universidad de Córdoba, Campus de Rabanales, Ed. Marie Curie, E-14071 Córdoba, Spain. q82calum@uco.es
[c] Dpto. de Química Inorgánica, Cristalografía y Mineralogía, Facultad de Ciencias, Universidad de Málaga, 29071, Málaga, Spain.
[d] Peoples Friendship University of Russia (RUDN University), 6 Miklukho-Maklaya str., 117198, Moscow, Russia.

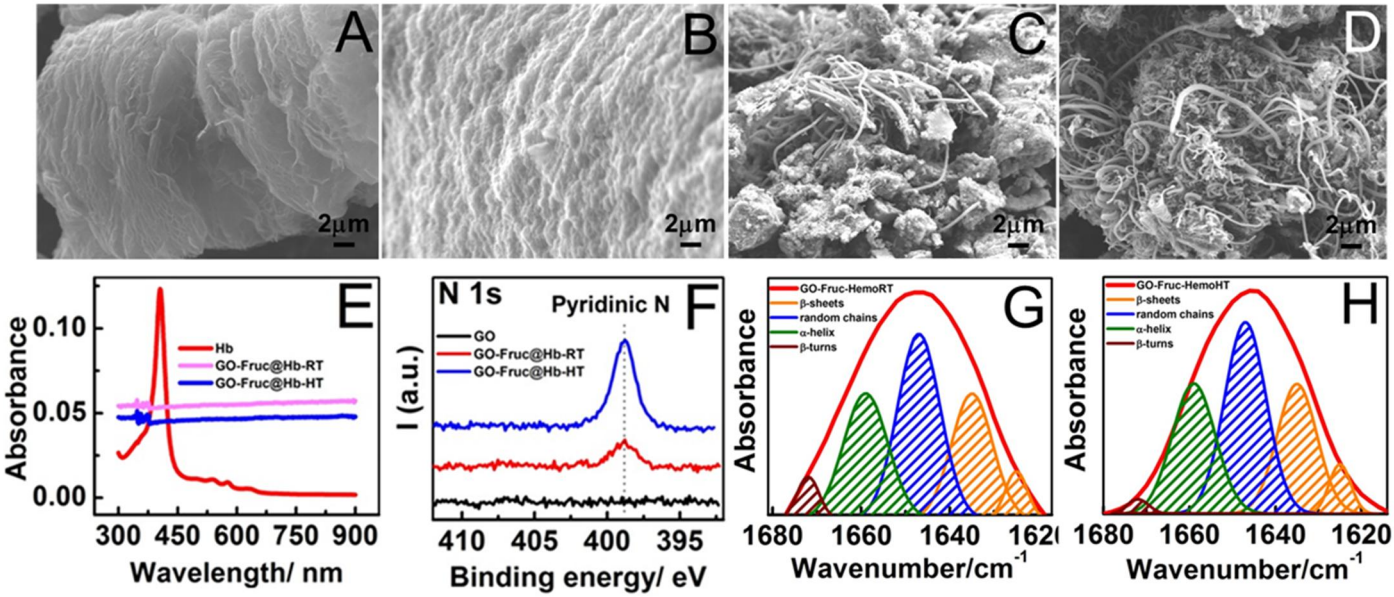

Fig. 1. SEM images of (A) GO, (B) GO-Fruc, (C) GO-Fruc@Hb-RT and (D) GO-Fruc@Hb-HT, respectively. (E) UV spectra of GO, GO-Fruc@Hb-RT and GO-Fruc@Hb-HT. (F) N1s XPS spectra of GO, GO-Fruc@Hb-RT and GO-Fruc@Hb-HT. Deconvoluted amide I bands of (G) GO-Fruc@Hb-RT and (H) GO-Fruc@Hb-HT, respectively.

GO-Fruc@Hb nanocomposites were synthesized by a novel methodology at room temperature and 80ºC. A 5 wt% graphene oxide solution was prepared using acetonitrile as a solvent. Then, the reaction was initiated by adding 10 mmol of fructose to the mixture. After 45 minutes of mixing, a hemoglobine aqueous solution ($5 \cdot 10^{-6}$ M) was added drop by drop to the reaction and it was left under continuous stirring at room temperature during 24h. The resulting material was then centrifuged and the supernatant was discarded. The pellet containing the synthesized biomaterial was resuspended into a fresh acetonitrile solution by a moderate shaking. This purification protocol was repeated three times to assure the complete removal of the physically adsorbed hemoglobins. Finally, the resulting nanobiomaterials were gently dried and stored until they were needed. It was named GO-Fruc@Hb-RT. To synthesize GO-Fruc@Hb-HT it was follow the same protocol described above. However after adding the hemoglobine solution it was transferred to a carrousel place station when remained under continuous stirring at 80ºC during 24 h. The final material was subjected to the same purification protocol. Therefore, the bottom-up strategy was divided in two steps. Firstly, the secondary hydroxyl groups of fructose were covalently linked to the epoxyde moieties on the GO surface by an epoxyde-hydroxyl reaction.[14, 15] Secondly, a glycan-protein interface was created by the surface linkage through a glycosidic bond of amino groups of superficial aminoacids residues and the O-linked glycans of the fructose.[16]

The synthesized nanobiostructures were characterized by a multitechnique approach with the aim to elucidate the structural and electrochemical properties of the redox enzymes covalently attached to GO-Fruc nanoplatforms.

Scanning electron microscopy (SEM) images were obtained for all relevant samples throughout the synthetic procedure (Fig. 1A-D). Fig. 1A shows a typical SEM image of the GO starting material with a layered- and exfoliated-structure.[17] After the epoxyde-hydroxyl reaction, the resulting GO-Fructose showed significant morphological changes with the appearance of homogeneous wrinkles and a more rippled structure (Fig. 1B). The subsequent addition of hemoglobin to the composites provides the formation of fibrin-like structures,[18] which were especially evident on the nanobiomaterials obtained at high temperatures and revealed a remarkable protein unfolding process upon the immobilization (GO-Fruc@Hb-RT, Fig.1D). Neither the starting GO material nor the GO-Fruc showed these fibrin-like structures, demonstrating the successful biofunctionalization of GO@Fruc nanoplatforms.

XPS measurements were carried out to study the chemical state of the elements on the surface of the prepared nanobiocomposites. The survey spectra of GO, GO-Fruc@Hb-RT and GO-Fruc@Hb-HT (Figure S1) revealed the presence of C and O in the case of GO, and the same elements plus N in the case of GO-Fruc@Hb-RT and GO-Fruc@Hb-HT. The N 1s core level spectra for GO, GO-Fruc@Hb-RT and GO-Fruc@Hb-HT (Figure 1F) show the presence of single peak at 398.9 eV for samples GO-Fruc@Hb-RT and GO-Fruc@Hb-HT. This binding energy is assigned to C-N=C groups (pyridinic N)[19, 20] and with a higher relative intensity in the case of GO-Fruc@Hb-HT. Consequently, the effectiveness of the Hb functionalization process was successfully confirmed. Table S1 shows the surface chemical composition for GO, GO-Fruc@Hb-RT and GO-Fruc@Hb-HT. The % of O increases for samples GO-Fruc@Hb-RT and GO-Fruc@Hb-HT due to the presence of fructose and Hb-protein at the composite surfaces. Surface N contents were estimated to be 0.56% and 1.6% for GO-Fruc@Hb-RT and GO-Fruc@Hb-HT, respectively, which are in the order of other N-doped GO@Hb nanocomposites.[21] Finally, it is observed a clear increase of the surface N content upon heating from 0.56 to 1.60% suggesting additional conformational changes in the GO-Fruc@Hb-HT structure.

A conformational analysis of the amide I band (Figure 1 G , H) of both nanobiomaterials was conducted to shed light over the secondary structure of the metalloenzymes covalently attached onto GO-Fruc nanoplatforms as well as their probable conformational distortion from the native-like structure. Native conformation of Hb contains 43% α-helix structures, 39% β-sheets and 18% turns. After conjugating with fructose@GO nanoplatforms via glycosylation reaction, the amount of the α-helix slowed down significantly with a concomitant increasing of β-sheet and random contents indicating striking conformational changes of Hb at the enzyme/GO-Fruc interfaces (Table S2).[22]

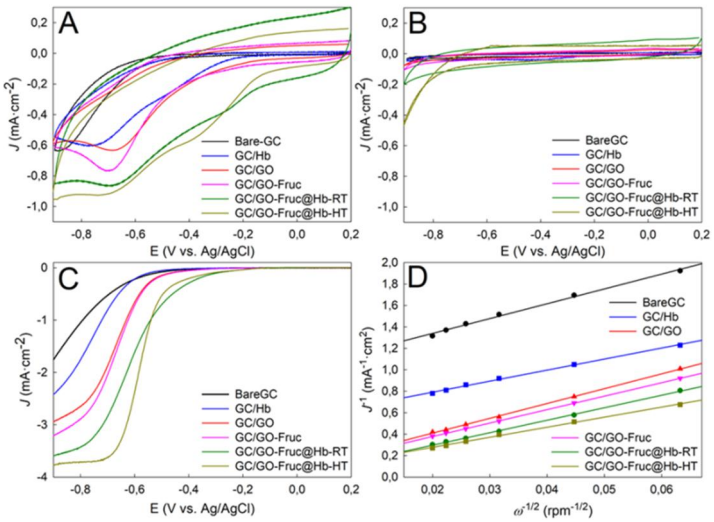

Figure 4. Cyclic voltammograms of GC electrodes unmodified and modified with hemoglobin (Hemo), Graphene Oxide (GO), GO-Fructose (GO-Fruc), GO-Fruc@Hb-RT and GO-Fruc@Hb-RT in O_2-saturated (A) and N_2-saturated (B) 0.1 M PBS (pH 7.2) at scan rate of 0.1 $V{\cdot}s^{-1}$. Rotating-disk voltammograms (RDVs) at rotation rate of 2500 rpm and scan rate of 0.01 $V{\cdot}s^{-1}$ (C) and Koutecky-Levich plots obtained from Figure S2, at -0.75 V (D), for all samples.

Importantly, the degree of conformational changes of Hb secondary structure, in which α-helix contents significantly decreased from 43% to 20% and β-sheets/random domains underwent a two-fold increase (Table S2), was slightly acute on the biomaterial obtained at 80°C, revealing the direct influence of temperature on the enzymes conformational arrangement. Additionally, UV-vis characterization of the nanobiocomposites (Figure 1E) showed the lack of the typical Soret band at 407 nm of hemoglobin, which clearly revealed the absent of heme groups in the immobilized enzymes. Consequently, it can be expected a large unfolding of hemoglobin 3D structure on the nanoplatforms as well as the rupture of the histidines coordination with the metalloprotein iron sites. In fact, Yaakov Levi and coworkers have demonstrated using all-atoms molecular dynamic simulations that glycosilation can induced significant conformational distortions over bonded proteins, preferentially α-helical rich proteins.[23] In summary, the remarkable structural and conformational changes at the protein/electrolyte interfaces may provide a high degree of accessibility to histidines towards the oxygen adsorption and therefore they will be able to work as molecular electrocatalytic machines through their catalytically active sites pyridine-like nitrogens.

After exhaustive characterization, the electrocatalytic properties of the different composites and their individual constituents were compared by electrochemical analysis in physiological conditions (0.1 M PBS buffer pH 7.2) using the oxygen reduction reaction (ORR) (Figure 4). For this, all samples were deposited by drop-casting, and subsequent drying, on the surface of a glassy carbon (GC) electrode. On the one hand, Figure 4A compares the electrocatalytic performance of the different modified and unmodified GC electrodes toward the ORR. For the unmodified GC electrode the peak potential was -0.90 V, the hemoglobin (hemo)-modified peak potential was –0.75 V, the pristine graphene oxide (GO)-modified -0.70 V, the composite GO-Fruc@Hb-RT -0.68 V and GO-Fruc@-HT -0.65 V. Both, potential shift to less negative values and current density maxima increase, were observed for the GO-Fruc@Hb composites, indicating an efficient ORR response of these materials and an extra-improvement of the enzyme electrocatalytic performance. Indeed, Figure 4B demonstrates that the corresponding ORR cathodic peaks were not presented under saturated N_2 environment. It is worth to note that unlike previous works,[24] the electrocatalytic performance of the covalently attached hemoglobins is not related with the iron active sites owed to they were totally removed from the protein structure after the immobilization process. Therefore, although the electron donating effect of amine groups of protein framework cannot be rule out, we attributed the main electrocatalytic response to the role of pyridine-like nitrogens belonging to histidine residues, which are disposed in highly accessible positions at the electrochemical interface and in turn are able to transform the neighboring carbon atoms (carbon atoms next to pyridinic N) in ORR highly efficient catalytically active sites. In this sense, Junji Nakamaru and coworkers, through a seminal work, have definitely clarified the mechanism for the ORR activity in N-doped carbon materials.[25] They demonstrated that pyridinic N can create carbon atoms with Lewis basicity, which are responsible of the suitable adsorption of O_2 molecules during the first step of the oxygen electroreduction.

On the other hand, to gain further insights into the ORR, rotating-disk voltammograms (RDVs) were acquired for the different modified and unmodified GC electrodes in oxygen-saturated 0.1 M PBS buffer (pH 7.2) electrolyte solution at different rotation rates, from 250 to 2500 rpm (Figure S2). As it was expected, the cathodic current density of all samples increases with increasing rotation rate. Figure 4C compares the resulting RDV curves for all samples at the same rotation rate of 2500 rpm. The shapes of the RDV-curves obtained for the three-component GO-Fructose-Hemoglobin composites were quite similar to the one reported previously for the multiwalled carbon nanotubes (MWCNTs) chemically functionalized with pyridine groups under mild reaction conditions.[26] Table 1 shows that ORR onset potentials measured for both three-component composite electrocatalysts (GO-Fruc@Hb-RT and GO-Fruc@Hb-HT) are shifted to more positive values than their individual components, thus featuring their higher electrocatalytic activities. In addition, an evident increase of the limiting current density can be observed for both composites, being the best electrocatalytic performance for the one prepared under higher temperature, which can be attributed to the increased number of superficial pyridinic N active sites induced by the additional conformational changes. Both the resulting onset potential and limiting current density values for the GO-Fruc-Hb composites were very close to the ones previously reported for pyridine functionalized MWCNTs[24] and even surpassed by far some of the most proficient N-doped nanocarbons obtained from proteins,[27] demonstrating both the suitability of this novel alternative approach and the strong influence of pyridine-like nitrogens belonging to histidine residues on the final electrocatalytic yields. Figure 4D shows the obtained Koutecky-Levich (K-L) plots from the Figure S2 at -0.75 V. The excellent linearity demonstrates first-order reaction toward dissolved O_2 for all samples. From the K-L plots on the basis of the K-L equations, the average number of electrons transferred (n) per oxygen molecule at -0.75 V was calculated (Table 1).[28] For instance, the n value of the GO-Fruc@Hb-HT composite was estimated to be 3.2 per O_2 molecule by using the values of oxygen concentration

of $8.8 \cdot 10^{-7}$ mol·cm^{-3}, O_2 diffusion coefficient of $2.7 \cdot 10^{-5}$ cm^2·s^{-1}, and kinematic viscosity of 0.01 cm^2·s^{-1} in 0.1 M PBS (pH 7.2).[29] The latter result suggests a nearby 4 electron pathways for this composite material, being remarkable the obtained n value for the oxygen reduction reaction at -0.75V in physiological environment.

Table 1. Onset potential values and average number of electrons transferred for O_2 molecules obtained at -0.75 V from Figures 4C and S2, respectively.

Catalysts	Onset potential (V)	Number of transferred electrons at 0.75V
GC	-0.324	2.1
Hemoglobin	-0.321	2.9
GO	-0.237	2.2
GO-Fructose	-0.237	2.4
GO-Fruc-HemoRT	-0.139	2.6
GO-Fruc-HemoHT	-0.139	3.2

Conclusions

The as-prepared electrocatalytically active biomaterials represent a completely new concept towards the utilization of unfolded proteins on nanosized carbons as high-performance ORR electrocatalysts. Importantly, these results pave the way towards the development of ORR biofuels cells cathodes with impressive catalytic performances from the use of fructose modified graphene structures as effective nanoplatforms to unfold the histidine residues of α-helical rich proteins and, in turn, boost their ORR electrocatalytic function.

Acknowledgements

Rafael Luque gratefully acknowledges MINECO for funding project CTQ2016-78289-P, co-financed with FEDER funds. Alain R. Puente-Santiago gratefully acknowledges MINECO for their research contracts associated to the aforementioned project. Ana Franco also thanks for an FPI contract (BES-2017-081560) under the framework of the granted proyect. Support from the Ministry of Economy and Competitiveness of Spain is acknowledged through the CTQ2017-83961-R project. J.J.G.-C. acknowledges the Ministry of Economy and Competitiveness for a "Ramon y Cajal" contract (#RyC-2014-14956). M. C. thanks the "Plan Propio de Investigación" from the Universidad de Córdoba (UCO) and the "Programa Operativo de fondos FEDER Andalucía" for its financial support through a postdoctoral contract (Modality 5.2.A). Enrique Rodríguez-Castellón thanks the Funding from CTQ2015–68951-C3-3-R (MINECO, Spain) and FEDER. The publication has been prepared with support from RUDN University Program 5-100.

References

1. Zhang, G. B. Chen, K. Mullen and X. L. Feng, *Adv. Mater.*, 2018, **30**, 1800528.
2. Y. P. Zhu, C. X. Guo, Y. Zheng and S. Z. Qiao, *Acc. Chem. Res.*, 2017, **50**, 915-923.
3. H. B. Tan, Y. Q. Li, X. F. Jiang, J. Tang, Z. L. Wang, H. Y. Qian, P. Mei, V. Malgras, Y. Bando and Y. Yamauchi, *Nano Energy*, 2017, **36**, 286-294.
4. X. L. Zhao, F. Li, R. N. Wang, J. M. Seo, H. J. Choi, S. M. Jung, J. Mahmood, I. Y. Jeon and J. B. Baek, *Adv. Funct. Mater.*, 2017, **27**, 1605717.
5. Z. Z. Liang, X. Fan, H. T. Lei, J. Qi, Y. Y. Li, J. P. Gao, M. L. Huo, H. T. Yuan, W. Zhang, H. P. Lin, H. Q. Zheng and R. Cao, *Angew. Chem. Int. Ed.*, 2018, **57**, 13187-13191.
6. Q. Lv, W. Y. Si, J. J. He, L. Sun, C. F. Zhang, N. Wang, Z. Yang, X. D. Li, X. Wang, W. Q. Deng, Y. Z. Long, C. S. Huang and Y. L. Li, *Nat. Commun.*, 2018, **9**, 3376.
7. Y. S. Zhao, J. W. Wan, H. Y. Yao, L. J. Zhang, K. F. Lin, L. Wang, N. L. Yang, D. B. Liu, L. Song, J. Zhu, L. Gu, L. Liu, H. J. Zhao, Y. L. Li and D. Wang, *Nat. Chem.*, 2018, **10**, 924-931.
8. Z. Y. Wu, X. X. Xu, B. C. Hu, H. W. Liang, Y. Lin, L. F. Chen and S. H. Yu, *Angew. Chem. Int. Ed.*, 2015, **54**, 8179-8183.
9. J. T. Zhang, Z. H. Zhao, Z. H. Xia and L. M. Dai, *Nat. Nanotechnol.*, 2015, **10**, 444-452.
10. K. G. Qu, Y. Zheng, S. Dai and S. Z. Qiao, *Nano Energy*, 2016, **19**, 373-381.
11. J. T. Jin, F. P. Pan, L. H. Jiang, X. G. Fu, A. M. Liang, Z. Y. Wei, J. Y. Zhang and G. Q. Sun, *ACS Nano*, 2014, **8**, 3313-3321.
12. S. K. Singh, K. Takeyasu and J. Nakamura, *Adv. Mater.*,2018, 1804297.
13. M. L. Feng and H. Tachikawa, *J. Am. Chem. Soc.*, 2001, **123**, 3013-3020.
14. M. Cano and G. de la Cueva-Mendez, *Chem. Commun.*, 2015, **51**, 3620-3622.
15. G. Nikolic, S. Zlatkovic, M. Cakic, S. Cakic, C. Lacnjevac and Z. Rajic, *Sensors*, 2010, **10**, 684-696.
16. D. Hemmler, C. Roullier-Gall, J. W. Marshall, M. Rychlik, A. J. Taylor and P. Schmitt-Kopplin, *Sci. Rep.*, 2018, **8**, 16879.
17. M. A. Velasco-Soto, S. A. Perez-Garcia, J. Alvarez-Quintana, Y. Cao, L. Nyborg and L. Licea-Jimenez, *Carbon*, 2015, **93**, 967-973.
18. L. D. Zubairova, R. M. Nabiullina, C. Nagaswami, Y. F. Zuev, I. G. Mustafin, R. I. Litvinov and J. W. Weisel, *Sci. Rep.*, 2015, **5**, 17611.
19. S. K. Bhunia, S. Dolai, H. C. Sun and R. Jelinek, *Sens. Actuator B-Chem.*, 2018, **270**, 223-230.
20. J. T. Yin, Z. Li, Y. Cai, Q. F. Zhang and W. Chen, *Chem. Commun.*, 2017, **53**, 9430-9433.
21. J. Lavanya, A. Subbiah, S. Neogi and N. Gomathi, Sens. Actuator B-Chem., 2018, **255**, 536-543.
22. Q. Shao, P. Wu, P. A. Gu, X. Q. Xu, H. Zhang and C. X. Cai, *J. Phys. Chem. B*, 2011, **115**, 8627-8637.
23. Y. Gavrilov, D. Shental-Bechor, H. M. Greenblatt and Y. Levy, *J. Phys. Chem. Lett.*, 2015, **6**, 3572-3577.
24. S. V. Sokolov, L. Sepunaru and R. G. Compton, *Appl. Mater. Today*, 2017, **7**, 82-90.
25. D. H. Guo, R. Shibuya, C. Akiba, S. Saji, T. Kondo and J. Nakamura, *Science*, 2016, **351**, 361-365.
26. G. Tuci, C. Zafferoni, A. Rossin, A. Milella, L. Luconi, M. Innocenti, L. T. Phuoc, D. V. Cuong, P. H. Cuong and G. Giambastian, *Chem. Mater*, 2014, **26**, 3460-3470.
27. C. Z. Guo, W. L. Liao, Z. B. Li, L. T. Sun and C. G. Chen, *Nanoscale*, 2015, **7**, 15990-15998.
28. D. A. Molina, A. R. P. Santiago, J. J. G. Casares, M. T. M. Romero, L. Camacho, R. Luque and M. Cano, *J. Phys. Chem. C*, 2019, under review
29. M. S. El-Deab, T. Okajima and T. Ohsaka, *J. Electrochem. Soc.*, 2003, **150**, A851-A857.

